



ISSN 0975-413X
CODEN (USA): PCHHAX

Der Pharma Chemica, 2016, 8(7):80-90
(<http://derpharmachemica.com/archive.html>)

Investigation on a cost effective bottom-up approach for developing core/shell $\text{Fe}_3\text{O}_4/\text{Ag}$ nanoparticles with enhanced optical and magnetic properties

S. Amala Jayanthi^a, D. Muthu Gnana Theresa Nathan^b, S. John Sundaram^b, R. Mahesh^b
Shibu Joseph^b and P. Sagayaraj^{b*}

^aDepartment of Physics, Government Arts College (Autonomous), Nandanam, Chennai-600 035, India

^bDepartment of Physics, Loyola College (Autonomous), Chennai -600 034. India

ABSTRACT

In the present work, an attempt has been made to coat the magnetic nanoparticles of iron oxide with the noble metal silver via a solvothermal approach. The synthesized particles are characterized by X-ray diffraction (XRD), Transmission Electron Microscopy (TEM) and Scanning Electron Microscopy (SEM). The optical and magnetic properties are investigated by UV-Vis-Spectrometer and Vibrating Sample Magnetometer (VSM). In the X-ray diffractogram, the absence of the peaks of iron and the presence of only the prominent peaks of silver confirmed the formation of iron oxide core/silver shell nanoparticles. The SEM image clearly indicates the coating of iron with silver. The Energy Dispersive X-ray Analyzer (EDX) spectrum evidences the high purity of the samples. The TEM images confirm the nanoparticles formation and the $\text{Fe}_3\text{O}_4/\text{Ag}$ core/shell structure. The UV spectrum and the magnetization curves indicate that the resulting samples have a modified optical and magnetic properties compared to the parent material.

Keywords: Iron oxides; Chemical synthesis; Nanocomposites; Electron microscopy; Magnetic property; Hysteresis

INTRODUCTION

Magnetic particles of nanometer scale are of great interest due to their technological applications. These particles with size approaching single magnetic domain find their applications in magnetic data storage, magnetic recording, biomedical field, etc., [1,2]. Particularly, in Magnetic Resonance Imaging (MRI) they can be exploited to provide effective contrast agents. Magnetite (Fe_3O_4) is an attractive material and due to its strong magnetic properties it has gained significant attention in biotechnology and bio-medicine. However, the iron oxide nanoparticles in its pure form are not stable and therefore need to be coated with stable metals. Especially, coating with noble metals such as gold (Au), silver (Ag) and platinum (Pt) is preferred due to their unique electronic and catalytic properties [3-5]. The resulting precious hybrid materials not only retain their individual magnetic, semiconducting and plasmonic properties but they also exhibit enhanced optical, magnetic and catalytic properties when compared with their individual single component materials [6].

In the present work, efforts have been made to coat the Fe_3O_4 nanoparticles with noble metal silver. From application point of view, coating with Ag is preferred because it is cheaper than Au and can be incorporated into products that range from photovoltaics to biological and chemical sensors [7-9]. An increasingly common

application of Ag nanoparticles is its employment for antimicrobial coatings and many textiles, keyboards and wound dressings. Biomedical devices now contain Ag nanoparticles that continuously release a low level of silver ions to provide protection against bacteria [10-13]. When the Ag nanoparticles were used to form hybrid material with the Fe₃O₄ nanoparticles, in addition to the above mentioned properties they acquire some magnetic properties, which make them special in biomedical applications.

There are a few interesting works reported in the literature which are related to the synthesis of hybrid nanomaterials involving Fe₃O₄ and Ag. Shichuan Li et al. (2014) have synthesized Ag/Fe₃O₄ nanocomposites by electroless silver plating technique and demonstrated that the inorganic magnetic nanocomposites possess excellent dielectric loss, good magnetic loss at 2 GHz to 5 GHz and also has infrared reflection characteristic [14]. Shujun Yu et al. (2013) have prepared an immunosensor with Ag/Fe₃O₄ nanoparticles and employed it for the detection of kanamycin [15]. Ling Chen et al. (2014) have reported high sensitivity for the detection molecular biothiols using the fluorescein isothiocyanate (FITC) functionalized magnetic core-shell Fe₃O₄/Ag hybrid nanoparticles [16]. Recently, Benyang Wang and Shiliang Qu (2014) have evaluated the electric field enhancement factors of Au and AgFe₃O₄ dimers and reported that the presence of the magnetite nanocube significantly alters the amplitude distribution of the enhanced electric field of the metal nanosphere especially, in Surface Plasmon Resonance (SPR) region [17].

Altangerel Amarjargal et al. (2013) have successfully prepared core-shell Ag/Fe₃O₄ nanocomposites by modified co-precipitation route followed by a facile hydrothermal treatment in one-pot synthesis without adding any reducing agent [18]. Zhang Ling Yan et al. (2013) have prepared Fe₃O₄-core@Ag-shell nanoeggs using thiol as capping agent and by reducing aliquots of AgNO₃ solution using NaBH₄ as a reducing agent. The as-prepared Fe₃O₄-core@Ag-shell nanoeggs are proposed to detect fingermarks on different surface, with which the fingermarks can be viewed directly due to the clear ridge detail [19]. Jum Suk Jang et al. (2009) have developed Ag/Fe₂O₃ nanocomposite photocatalysts and proved that the improved conductivity of Fe₂O₃ was due to the presence of Ag metal [20]. E. Iglesias Silva, et al. (2007) have synthesized silver coated magnetite nanoparticles by microemulsion technique and observed a large decrease in the magnetization for the Ag coated Fe₃O₄ nanoparticles as compared to the pure Fe₃O₄ nanoparticles [21].

In this work, a simple co-precipitation method has been adopted to synthesize silver and Fe₃O₄ nanoparticles separately. The nanoparticles suspension is then mixed and subjected to solvothermal treatment to obtain the hybrid Fe₃O₄/Ag nanoparticles using common precursors. The synthesis procedure employed a non-toxic and bio-friendly reducing agent (glucose) for coating the Fe₃O₄ NPs. The synthesized nanoparticles are characterized by powder XRD, SEM and TEM. The optical properties are studied by UV-Vis and FT-IR spectroscopic techniques and the magnetic measurements are taken with VSM. The hybrid nanoparticles prepared by our method are of high purity, noble in character due to its coating by silver and are magnetic even after coating with silver and exhibit good optical behavior.

MATERIALS AND METHODS

2.1 Chemicals used

FeCl₃, AgNO₃, ethanol, urea, NaOH, PEG and chloroform were purchased from Merck Specialties Pvt. Ltd., Mumbai and FeCl₂·4H₂O was purchased from LOBA CHEMIE, Pvt. Ltd., Chennai. They were used as received without further purification.

2.2 Experimental

2.2.1 Synthesis of Fe₃O₄ nanoparticles

A simple co-precipitation method was used to prepare the Fe₃O₄ nanoparticles. FeCl₃ and FeCl₂·4H₂O were taken in the ratio of 2:1 and then dissolved in 100 ml of Millipore water. The solution was stirred for 15 min and then the pH of the solution was adjusted to 9 by the drop-wise addition of NaOH. It resulted in the formation of a black precipitate and thus confirmed the formation of Fe₃O₄ nanoparticles. By employing this procedure, 5 mM of aqueous solution of Fe₃O₄ nanoparticles was prepared. The resulting solution was labeled as A.

2.2.2 Synthesis of Ag nanoparticles

Aqueous solution of Ag was prepared in two different molar concentrations (10 mM and 20 mM) using the co-precipitation method. In order to prepare 10 mM of Ag, a solution with 10 ml of AgNO₃ was taken and 5 ml of urea was slowly added. The resulting solution was mixed with 4% PEG 4000 and then 20 mM of glucose solution was

added drop wise. NaOH solution was also added drop wise till an aqueous solution of Ag in nanoform is formed. Similar procedure was adopted for the preparation of 20 mM of Ag solution. The 10 mM and 20 mM aqueous solutions of Ag were taken as solution B and C, respectively.

2.2.3 Synthesis of Fe_3O_4/Ag nanocomposites

Solution A was poured into solution B and stirred gently for about 15 min. The resulting black colored solution was then transferred to a Teflon-lined autoclave. Two samples were prepared. In the first case, the molar ratio of Fe_3O_4/Ag was kept as 1:2. For the second sample, the molar ratio of Fe_3O_4 and Ag was maintained as 1:4. Solution A was poured into solution C and stirred for a few minutes, it was then transferred into another Teflon-lined autoclave. Both the autoclaves were kept in the furnace at 250° C for 4 h, then the autoclaves were cooled to room temperature and the products were washed with water and centrifuged. The samples collected from the first and second autoclaves were labeled as AgFNP1 and AgFNP2, respectively.

2.3 Characterization techniques

The powder XRD patterns for the as-prepared hybrid NPs were recorded by a Rich Seifert, X-ray diffractometer using monochromatic nickel filtered CuK_{α} ($\lambda = 1.5416 \text{ \AA}$) radiation. The optical property was studied from the absorption spectrum in the spectral region of 200 to 800 nm, using a UV-Vis-NIR VARIAN CARY 5E spectrophotometer. Perkin Elmer Spectrum FT-IR instrument was employed for recording the FT-IR spectrum. Freshly prepared nanopowder was mixed with KBr and pelletized using a hydraulic press and then the spectrum was recorded in the wavelength ranging from 450 to 4000 cm^{-1} . Scanning electron microscopic (SEM) analysis was performed using a JEOL JSM 6310 operated at 10 kV, CARL ZEISS SIPRA 55 Field Emission Scanning Electron Microscope (FESEM) that can be operated at various voltages from 0.5 kV to 20 kV with Energy Dispersive X-ray Analyzer (EDX) was also employed for morphological study and elemental analysis. The morphology and size of the NPs were determined from the TEM images recorded on a JOEL JEM 3010 at an accelerating voltage of 80 kV. Magnetic measurements were carried out with the Lake Shore Cryotronics, Inc. Vibrating Sample Magnetometer (VSM).

RESULTS AND DISCUSSION

3.1 X-ray diffraction study

The formation of the hybrid Fe_3O_4/Ag NPs of AgFNP1 and AgFNP2 nanoparticle was confirmed by the powder XRD diffractograms (Fig. 1a and b). All the prominent peaks at the respective 2θ values of 38.1625°, 44.3314°, 64.4467° and 77.4078° can be conveniently indexed to the (111), (200), (220) and (311) planes of zero-valent silver having face centered cubic structure with space group Fm3m (JCPDS card no : 044-0783). The crystallite size for both the samples was estimated based on the full width half maximum values of the (111) and (200) peaks using the Scherrer equation. The fact that the diffraction peaks for Fe_3O_4 are observed to be weak and less prominent than the Ag peaks is a strong evidence for the complete coverage of the Fe_3O_4 particles by AgNPs supporting the formation of Fe_3O_4/Ag core-shell NPs. In an earlier work, Xian Ming Liu and Ying Shun Li (2009) have also obtained low strength of Fe_3O_4 reflection in the XRD pattern and reported that it is due to the heavy atom effect arising from silver [22].

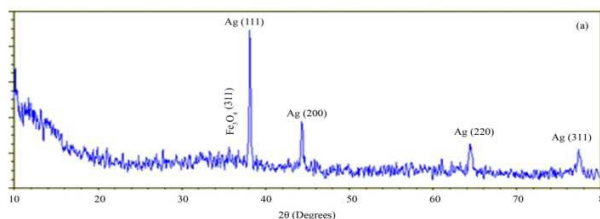


Figure 1(a) Powder XRD pattern of AgFNP1

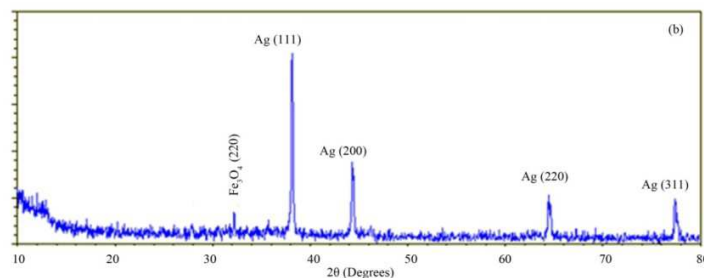
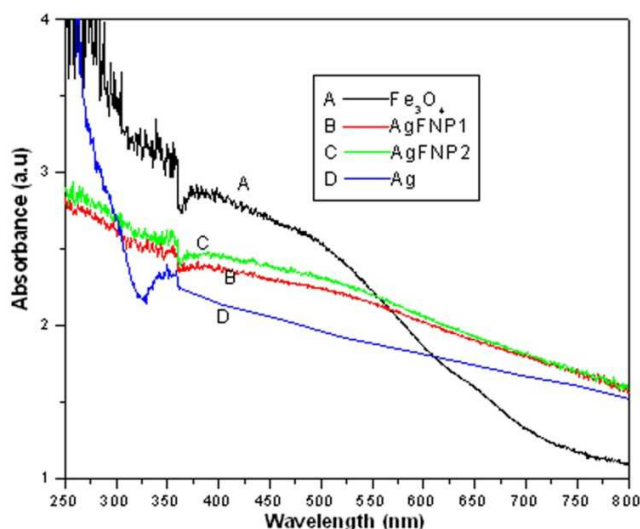


Figure 1(b) Powder XRD pattern of AgFNP2

3.2 UV-Vis Absorption Spectroscopy

Figure 2 depicts the UV-vis absorption spectra for bare Ag and bare Fe_3O_4 NPs along with AgFNP1 and AgFNP2 nanocomposites. It is evident from the spectra that the bare Ag NPs possess low absorption whereas, the bare Fe_3O_4 NPs exhibit high optical absorption. Interestingly, the $\text{Fe}_3\text{O}_4/\text{Ag}$ nanocomposites possess an intermediate level of optical absorption. For pure Ag NPs, the absorption peak corresponding to the SPR is observed at 355 nm in the near UV region. In the case of Ag coated nanoparticles, the absorption peaks positioned at 375 nm and 365 nm are due to the Ag SPR band, confirming the presence of silver in both the AgFNP1 and AgFNP2 nanocomposites. This band is shifted to a higher wavelength in comparison with pure Ag NPs (355 nm). Similar such SPR band red shift phenomena had been reported for $\text{Fe}_3\text{O}_4/\text{Ag}$ nanocomposites by a few research groups [23-25]. This result could be due to the charge transfer between Ag NPs and the Fe_3O_4 NPs in a nanocomposite system. Thus the tuning of the SPR red shift could open the door to the development of advanced materials [23]. Further, the influence of particle size on SPR absorption of Ag changing from violet to the red end of the spectrum has been investigated in the past. As the particle size increases, the peak plasmon resonance shifts to longer wavelengths and broadens. Accordingly, when the particle size becomes greater than 80 nm, in the UV-vis absorption spectrum, a secondary peak is visible at a shorter wavelength than the primary peak. However, in the present investigation, we could observe only a single sharp peak. Thus, the observance of SPR absorption at 350 nm in our samples indicates that the size of the AgNPs is below 10 nm, this is also evident from our TEM result. Thus the optical absorption study of the nanocomposites prepared in this work proves that the optical property of Ag being induced into the Fe_3O_4 NPs.

Figure 2 UV-Vis absorption spectrum of Fe_3O_4 , Ag, AgFNP1 and AgFNP2

3.3 FT-IR analysis

In the FT-IR spectra (Figure 3a and b) of AgFNP1 and AgFNP2, the band around 3400 cm^{-1} is due to the $-\text{OH}$ stretching vibration corresponding to adsorbed OH on Ag coated Fe_3O_4 nanoparticles [26]. The band seen around

570 cm^{-1} is attributed to the stretching vibration of Fe-O [27]. The peak positioned at 1610 cm^{-1} represents the vibrating peaks of OH functional group of the PEG. The band between 1050-1070 cm^{-1} is due to C-O-C stretching [28]. The bands between 1750 to 500 cm^{-1} are generally due to C-O, C-C and Fe-O vibrations [29]. The peak observed at 2930 cm^{-1} can be assigned to -CH stretching [28]. It is well known that Ag nanoparticles do not have absorption in IR region [30]. Due to Ag nanoparticles coating, a new band around 940 cm^{-1} is seen which implies the formation of Ag/Fe₃O₄ nanocomposites.

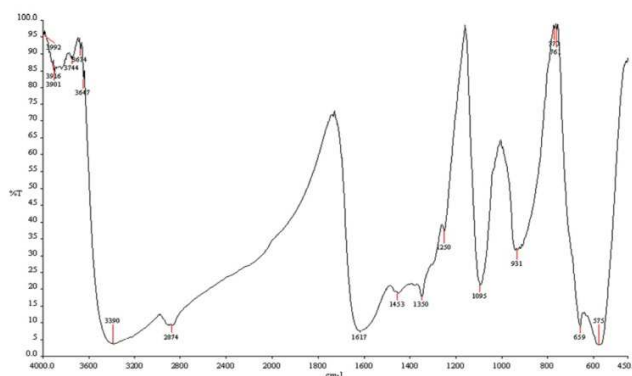


Figure 3 (a) FT-IR spectrum of AgFNP1

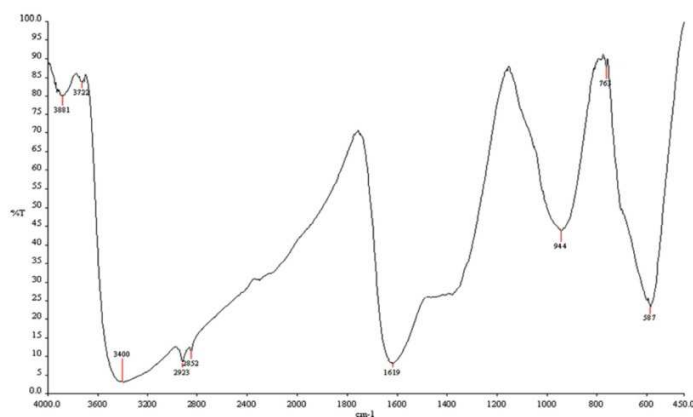


Figure 3 (b) FT-IR spectrum of AgFNP2

3.4 SEM and EDX analysis

To further confirm the formation of AgFNP1 and AgFNP2 hybrid nanocomposites, the typical surface morphology was examined by SEM. The elemental composition of the nanocomposites was determined from the EDX spectra collected during the SEM imaging. Figures 4a and b illustrates the SEM images and EDX spectra of AgFNP1 and AgFNP2. The micrographs reveal that surface of the composites is not glossy, indicating that silver nanoparticles are attached to Fe₃O₄ nanospheres. The tiny spherical Ag NPs are adhered uniformly on to the surface of large spherical aggregates of Fe₃O₄ NPs. One could clearly visualize from the bright spots in the SEM micrographs that there are two different NPs welded together.

The EDX spectra of the samples confirmed the elemental signature in the composite. The EDX spectra (Fig. 4) of AgFNP1 nanocomposites identify the 83.24% of Fe₃O₄ and 16.76% of Ag by mass and thus confirming the high purity of the sample. However, the EDX spectra (Fig. 5) recorded with FESEM shows nearly 1% impurity for the same sample. The inclusion of impurity during the preparation of Ag/Fe₃O₄ nanocomposites has been reported in the literature and samples containing more than 6-8% impurity were obtained [19,22,31]. Thus the present investigation demonstrates the high purity of the nanocomposites synthesized via co-precipitation coupled with hydrothermal approach. In the AgFNP2 nanocomposites, the percentage of Ag is found to be more due to the reason that the concentration of Ag was initially higher and the level of coating is also better in this sample.

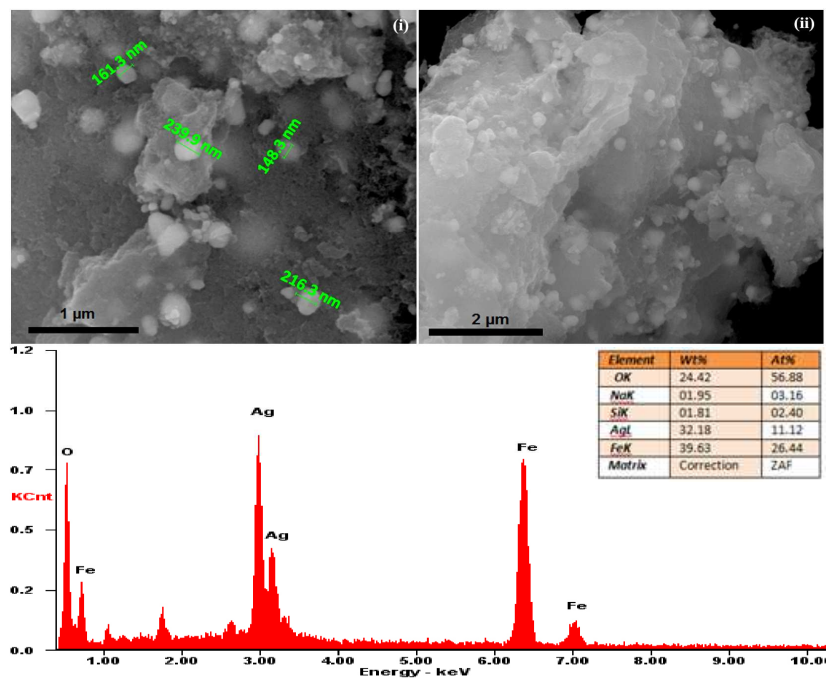


Figure 4 (a) SEM images and EDX spectrum of AgFNP1

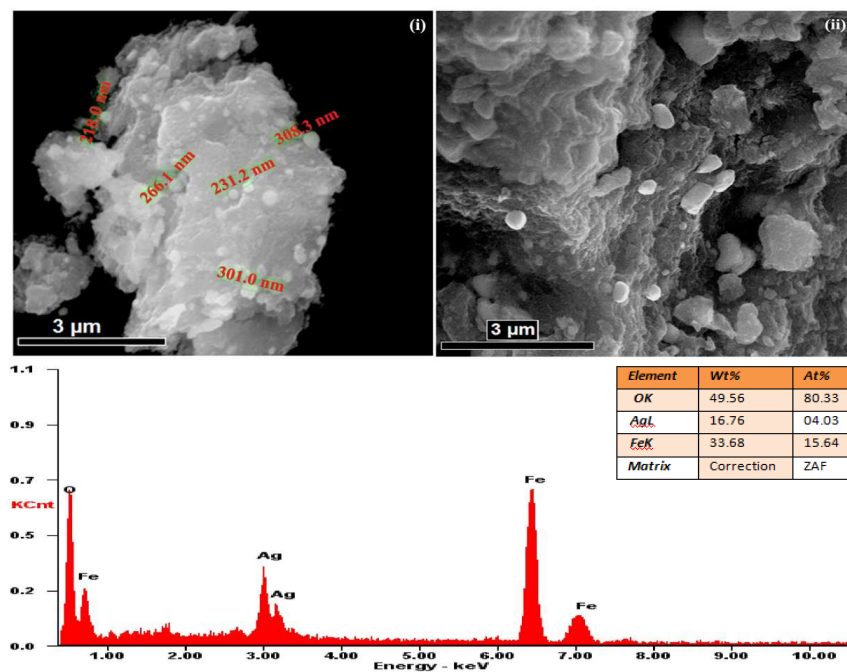


Figure 4 (b) SEM images and EDX spectrum of AgFNP2

3.5 FESEM and EDX analysis

Figure 5a shows the FESEM images AgFNP1 and AgFNP2 nanocomposites. It is noticed from the images that there is no unwrapped core or separate irregular particles, which indicates the homogenous distribution of two phases. The observed FESEM images provide evidence for the formation of tiny spherical aggregates as well as larger spherical aggregates. The uses of ferrous salt and AgNO₃ have led to the formation of fine nanocomposite particles of high dispersion with spherical morphology [18].

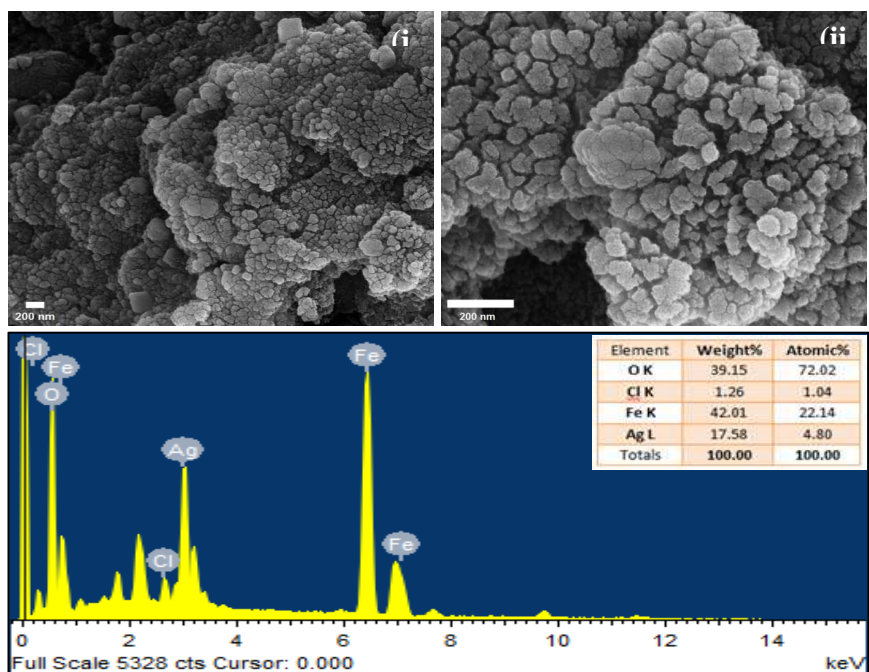


Figure 5 (a) FESEM images and EDX spectrum of AgFNP1

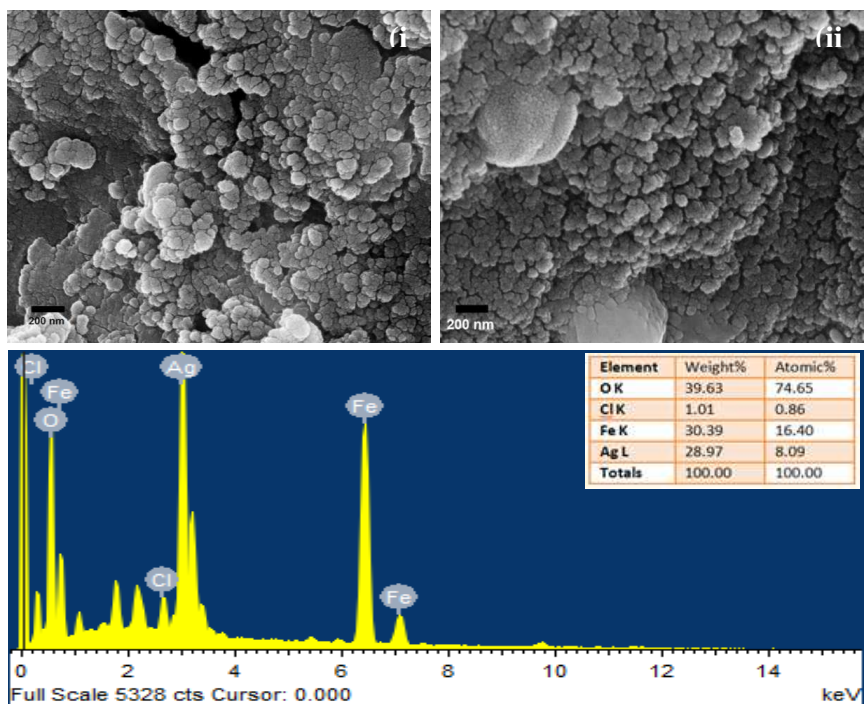


Figure 5 (b) FESEM images and EDX spectrum of AgFNP2

3.6 TEM analysis

The morphology and the size of AgFNP1 and AgFNP2 were further examined by TEM. Figures 6a and 7b show the TEM images of the samples at two different magnifications. Liquid (water) suspensions of the samples were dropped on to the form various coated grids. The images clearly illustrate the formation of quantum dots. The dark colored nanoparticles represent the Fe₃O₄ nanoparticles coated with Ag nanoparticles and the bright ones indicate

uncoated Fe_3O_4 nanoparticles. Both Fe_3O_4 and Ag crystallize in fcc structure and are spherical and thereby favors the formation of Ag shell over the Fe_3O_4 core. In AgFNP2 sample, the proportion of Ag is more, as a result the silver layer grows well over the Fe_3O_4 core. The size of the core is found to be around 4 nm and 5 nm for the AgFNP1 and AgFNP2 nanocomposites.

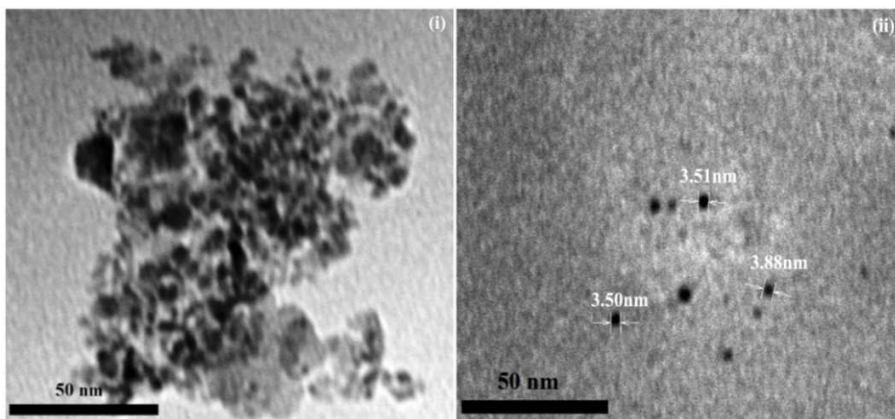


Figure 6 (a) TEM images of AgFNP1

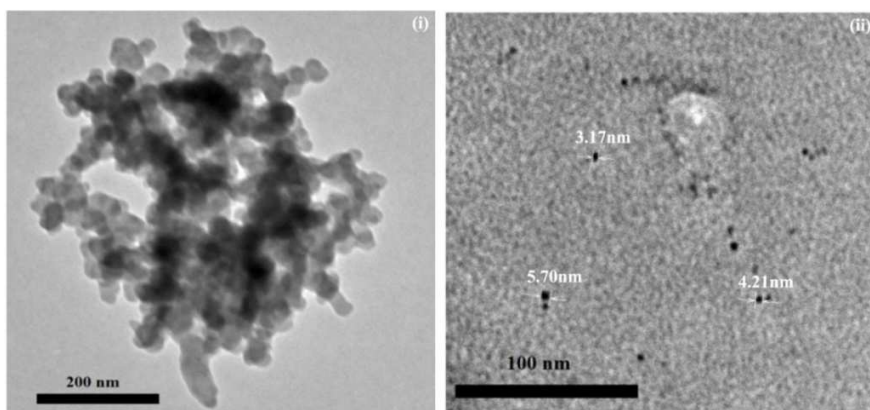


Figure 6 (b) TEM images of AgFNP2

3.7 Magnetic Characterization

The M-H curves recorded at various temperatures (50K, 100K, 150K and 200K) and the ZFC-FC magnetization curves for AgFNP1 and AgFNP2 are shown in Figures 7 and 8. The room temperature M-H curves for the bare Fe_3O_4 along with AgFNP1 and AgFNP2 nanoparticles are also shown in Fig. 9. The nanocomposites exhibit ferromagnetic behavior with M_s values of 6.7585 emu/g and 2.9 emu/g (at room temperature) for AgFNP1 and AgFNP2, respectively. A clear decrease in the saturation magnetization of at least 5 times smaller than the bare iron oxide nanoparticles is evident for the Ag coated nanoparticles. The decrease in the saturation magnetization for both the AgFNP1 and AgFNP2 nanoparticles as compared to the bare Fe_3O_4 nanoparticles is due to the contribution of the silver nanoparticles to the overall mass. It may also be considered as a result of decrease in the magnetic surface anisotropy (K_s) due to the coating formed by the silver nanoparticles. E. Iglesias-Silva *et al.* (2007) have synthesized silver coated magnetic nanoparticles and obtained similar such results [21]. Only a slight decrease in the saturation magnetization was observed in the silver coated magnetic nanoparticles synthesized by Mahuri Mandal *et al.* (2005) [32]. Youyi Sun *et al.* (2011) have synthesized $\text{Fe}_2\text{O}_3/\text{Ag}$ core-shell composite nanoparticles with M_s values of 1.25 emu/g and 0.96 emu/g for $\alpha\text{-Fe}_2\text{O}_3$ and $\alpha\text{-Fe}_2\text{O}_3/\text{Ag}$ composite nanoparticles, respectively [31].

Also, from the curves it is seen that the saturation magnetization (M_s) for both the samples decrease as the room temperature is approached. It is also seen that as the temperature increases, the values of the coercivity and the retentivity decrease but do not attain the zero value. Further from the ZFC and FC plots, it is evident that both the

curves diverge near the room temperature and the block temperature is near the room temperature. It may be possible to get the absence of hysteresis above the room temperature. Thus our result indicates that the coating of the noble metal Ag on Fe₃O₄ nanoparticles modifies its magnetic property.

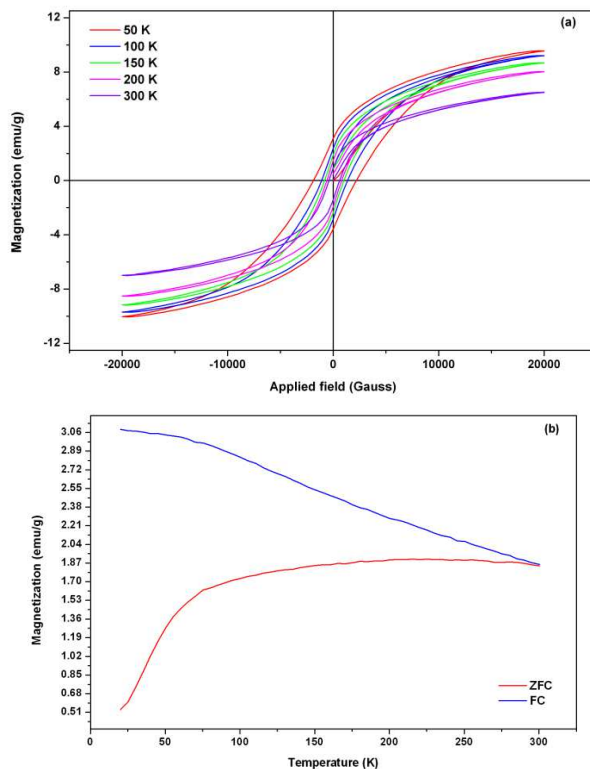


Figure 7 (a) M-H curves at different temperatures and (b) ZFC-FC magnetization curves for AgFNP1

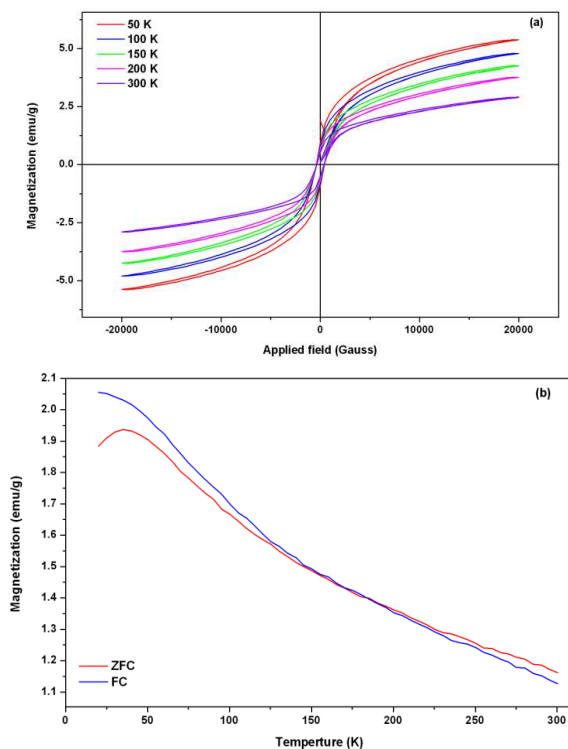


Figure 8 (a) M-H curves at different temperatures and (b) ZFC-FC magnetization curves for AgFNP2

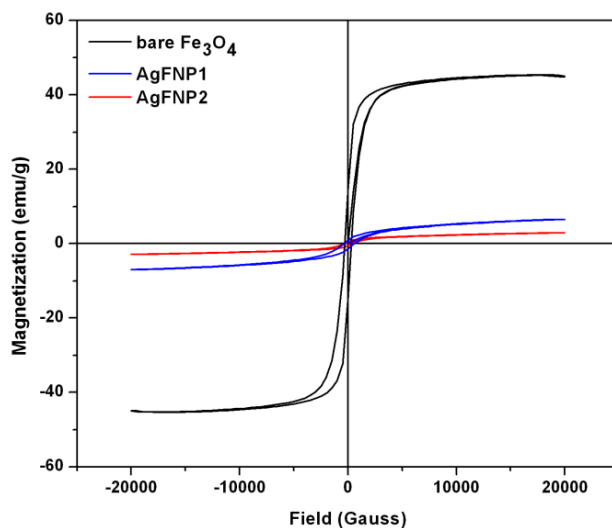


Figure 9 Room temperature M-H curves for bare Fe₃O₄, AgFNP1 and AgFNP2

Table 1 Saturation magnetization, retentivity and coercivity values at different temperatures

Sample	Temperature (K)	M _s (emu/g)	Retentivity (emu/g)	Coercivity (Gauss)
Bare Fe ₃ O ₄	50	44.768	18.780	664.49
	100	44.616	17.831	607.77
	150	44.507	17.512	585.63
	200	44.325	16.626	543.15
	300	40.300	13.130	381.63
AgFNP1	50	9.801	3.329	2033.80
	100	9.452	2.593	1227.10
	150	8.928	2.108	909.38
	200	8.270	1.700	696.15
	300	6.759	1.174	492.37
AgFNP2	50	5.385	0.936	406.48
	100	4.802	0.778	385.80
	150	4.260	0.687	382.32
	200	3.765	0.615	377.35
	300	2.900	0.517	371.91

CONCLUSION

A facile and efficient co-precipitation method followed by solvothermal approach was successfully developed for coating Ag noble metal over Fe₃O₄ NPs. XRD and TEM results authenticated the nanosize of the particles and their coatings. The SEM pictures along with the EDX spectrum show the coatings of the Fe₃O₄ with silver and confirmed the high purity of the synthesized nanocomposites. The VSM studies reveal that the magnetic property changes significantly for the Ag coated particles in comparison to that of the parent Fe₃O₄ NPs. The structural and elemental analysis along with the optical and electron microscopy studies confirms a near core-shell Fe₃O₄/Ag nanocomposite formation. Further, the magnetic and optical studies ascertain that the nanocomposites of AgFNP1 and AgFNP2 are optically and magnetically active materials. The nanocomposites synthesized in this work have the combination of good magnetic properties with optical characteristic and hence they will serve as useful material for application as a recyclable magnetic carrier with antimicrobial and catalytic properties.

Acknowledgement

The authors acknowledge Loyola College-Times of India (LC-TOI) Research initiative (Ref.No.3LCTOI14PHY001) for funding this research work and for providing the research facility at Department of Physics, Loyola College (Autonomous), Chennai -600034.

REFERENCES

- [1] T.C. Lin, F.H. Lin, J.C. Lin, *Acta Biomater.* **2012**, 8, 2704-2711.
- [2] L. Lou, K. Yu, Z.L. Zhang, R. Huang, J.Z. Zhu, Y.T. Wang, Z.Q. Zhu, *Nano Res.* **2012**, 5(4), 272-282.
- [3] K. Jiang, H.X. Zhang, Y.Y. Yang, R. Mothes, H. Lang, W.B. Cai, *Chem. Commun.* **2011**, 47, 11924-11926.
- [4] Y. Chi, Q. Yuan, Y. Li, J. Tu, L. Zhao, N. Li, X. Li, *J. Colloid Interface Sci.* **2012**, 383, 96-102.
- [5] L. Pan, T Jing, C. YongHong, *Sci China Chem.* **2013**, 56(3), 362-369.
- [6] M. Norsuria, J. Hua, H. Oleg, S. Outi, H. Simo-Pekka, *J. Nanopart. Res.* **2012**, 14, 987.
- [7] F. Raheman, S. Deshmukh, A. Ingle, A. Gade, M. Rai, *Nano Biomed. Eng.* **2011**, 3(3), 174-178.
- [8] Y. Shujun, W. Qin, D. Bin, W. Dan, L. He, Y. Liangguo, M. Hongmin, Z. Yong, *Biosensors and Bioelectronics*, **2013**, 48, 224-229.
- [9] C. Ling, L. Jinhua, W. Shasha, L. Wenhui, W. Aiguo, C. Jaebum, C. Lingxin, *Sensors and Actuators B: Chemical*, **2014**, 193, 857-863.
- [10] M. Zdenka, Š. Karolína Machalová, F. Jan, Č Jan, K. Milan, Š. Klára, M. Ivo, Z. Radek, *Environ. Sci. Technol.*, **2013**, 47(10), 5285-5293.
- [11] N. Gordon, L. Xuan, M. Sharifeh, M. Eric, E. James, *Materials Letters*, **2011**, 65(8), 1191-1193.
- [12] L. Jianguo, H. Baling, L. Xiangyou, L. Ping, Z. Xiaoyan, *J Electronic materials*, **2010**, 39(12), 2702-2710.
- [13] R. C. Jau, H. L. Bo, C. H. Kai, H. C. Dong, *J Hazardous Materials*, **2013**, 248-249, 394- 400.
- [14] L. Shichuan, Z. Zunning, Z. Tonglai, J. Guotao, S. Ruyi, *J Magnetism and Magnetic Materials*, **2014**, 358, 27-31.
- [15] Y. Shujun, W. Qin, D. Bin, W. Dan, L. He, Y. Liangguo, M. Hongmin, Z. Yong, *Biosensors and Bioelectronics*, **2013**, 48, 224-229.
- [16] C. Ling, L. Jinhua, W. Shasha, L. Wenhui, W. Aiguo, C. Jaebum, C. Lingxin, *Sensors and Actuators B: Chemical*, **2014**, 193, 857-863.
- [17] W. Benyang, Q. Shiliang, *Applied Surface Science*, **2014**, 292, 1002-1008.
- [18] A. Altangerel, D. T. Leonard, T. I. Ik, S. K. Cheol, *Chemical Engineering Journal*, **2013**, 226, 243-254.
- [19] L. Zhang, X. Zhou, T. Chu, *Science China, Chemistry*, **2013**, 56(5), 551-556.
- [20] S. J. Jum, Y. Y. Ki, X. Xiaoyin, R. F. F. Fu, B. Allen, *Chem. Mater*, **2009**, 21(20), 4803-4810.
- [21] E. Iglesias-Silva, J. Rivas, L.M. Leon Isidro, M.A. Lopez-Quintela, *J Non-Crystalline Solids* **2007**, 353 (8), 829-831.
- [22] L. Xian-Ming, L. Ying-Shun, *Materials Science and Engineering C*, **2009**, 29(4), 1128-1132.
- [23] Z. Ling, D. Yong-Hua, G. Hong-Chen, *J Colloid and Interface Science*, **2006**, 297, 660-664.
- [24] Y. Xuegang, W. Jiaqi, S. Yan, C. Kezheng, H. Xiaodong, *Chem. Mater*, **2009**, 21(20), 4892-4898.
- [25] Lingyan, Lingyan, L. Jin, F. Quan, S. Masatsugu, S. S. Itsuko, H. E. Mark, L. Yuehe, K. Nam, Q. W. Jian, J. Z. Chuan, *J. Phys. Chem. B*, **2005**, 109(46), 21593-21601.
- [26] K. Petcharoen, A. Sirivat, *Mater. Sci. Eng. B.*, **2012**, 177(5), 421-427.
- [27] S. Youyi, Y. Binghua, T. Ye, G. Guizhen, C. Wei, H. Minghong, L. Yaqing, *Micro & Nano letters*, **2011**, 6, 82-85.
- [28] A. S. Saqlain, A. Majeed, K. Rashid, A. Saif-Ullah, *Materials Chemistry and Physics*, **2013**, 138(2-3), 703-708.
- [29] C. Shao-Wen, Z. Ying-Jie, M. Ming-Yan, L. Liang, Z. Ling, *J. Phys. Chem. C.*, **2008**, 112(6) 1851-1856.
- [30] Y. Chi, Q. Yuan, Y.J. Li, J.C. Tu, L. Zhao, N. Li, X.T. Li, *J. Colloid Interf. Sci.* **2012**, 383(11) 96-102.
- [31] Y. Sun, G. Guo, B. Yang, X. Zhou, Y. Liu, G. Zhao, *J Non-Crystalline Solids*, **2011**, 357, 1085-1089.
- [32] M. Madhuri, K. Subrata, G. Sujit Kumar, P. Sudipa, K.S. Tapan, S.M.Yusuf, Tarasankar Pal, *J Colloid Interf Sci*, **2005**, 286(1), 187-194.